Magnetic structure and multiferroic coupling in pyroxene $NaFeSi_2O_6$

M. Baum,[1,*] A. C. Komarek,[1,†] S. Holbein,[1] M. T. Fernández-Díaz,[2] G. André,[3] A. Hiess,[2,‡] Y. Sidis,[3] P. Steffens,[2] P. Becker,[4] L. Bohatý,[4] and M. Braden[1,§]

[1]*II. Physikalisches Institut, Universität zu Köln, Zülpicher Straße 77, D-50937 Köln, Germany*

[2]*Institut Laue-Langevin, BP 156, 38042 Grenoble Cedex 9, France*

[3]*Laboratoire Léon Brillouin, C.E.A./C.N.R.S., F-91191 Gif-sur-Yvette CEDEX, France*

[4]*Institut für Kristallographie, Universität zu Köln, Greinstr. 6, 50939 Köln, Germany*

(Received 26 March 2015; revised manuscript received 12 May 2015; published 9 June 2015)

By comprehensive neutron diffraction measurements we have studied the magnetic structure of aegirine ($NaFeSi_2O_6$) in and above its multiferroic phase. Natural aegirine exhibits two magnetic transitions into incommensurate magnetic order with a propagation vector of $\vec{k}_{inc} = (0, \sim 0.78, 0)$. Between 9 and 6 K, we find a transverse spin-density wave with moments pointing near the c direction. Below 6 K, magnetic order becomes helical and spins rotate in the ac plane. The same irreducible representation is involved in the two successive transitions. In addition, the ferroelectric polarization $\vec{P}$ appearing along the b direction cannot be described by the most common multiferroic mechanism but follows $\vec{P} \propto \vec{S}_i \times \vec{S}_j$. Synthetic $NaFeSi_2O_6$ does not exhibit the pure incommensurate helical order but shows coexistence of this order with a commensurate magnetic structure. By applying moderate pressure to natural aegirine, we find that the incommensurate magnetic ordering partially transforms to the commensurate one, underlining the nearly degenerate character of the two types of order in $NaFeSi_2O_6$.

DOI: 10.1103/PhysRevB.91.214415 PACS number(s): 61.05.F−, 75.85.+t, 75.25.−j

I. INTRODUCTION

In the recently discovered multiferroic materials the ferroelectric polarization not only coexists with magnetic order, but is directly caused by the complex magnetic structure [1,2]. These materials are interesting in view of both applied and fundamental issues. For most of these multiferroic phases the ferroelectric polarization arises from a noncollinear magnetic order through the antisymmetric Dzyaloshinski-Moriya (DM) interaction [3]. The DM interaction usually describes the spin canting leading, for example, to weak ferromagnetism in a low-symmetry structure. Here, the spin canting arises through some other mechanism such as frustration and induces the structural distortion [3] which may result in a net ferroelectric polarization. This effect is described by $\vec{P}_I \propto \vec{r}_{ij} \times (\vec{S}_i \times \vec{S}_j)$, where $\vec{r}_{ij}$ is the connecting vector between two neighboring spins $\vec{S}_i$ and $\vec{S}_j$. This entity transforms as a polar vector and does well explain the ferroelectric polarization in many multiferroic materials such as $TbMnO_3$ [4], $Ni_3V_2O_8$ [5], and $MnWO_4$ [6–8]. This magnetoelectric coupling further results in a new type of collective excitation with mixed magnon phonon character which is labeled electromagnon [9–12] although there are also other sources of electromagnon scattering in $REMnO_3$ [13]. There can, however, exist other forms of canted-spin-caused electric dipoles, which may induce ferroelectric polarization. Kaplan and Mahanti analyzed these quadratic spin forms in general and found additional forms based on spin canting [14]. These additional forms, however, may only appear in the case of low symmetries. This analysis resembles the one for antisymmetric DM interaction $\vec{D} \cdot (\vec{S}_i \times \vec{S}_j)$ where symmetry fixes the possible orientation of the D vector [15]. For example, one of these additional forms $\vec{P}_{II} \propto (\vec{S}_i \times \vec{S}_j)$ does explain the ferroelectric polarization in $CuFeO_2$ [16,17], $CuCrO_2$ [18], and $RbFe(MoO_4)_2$ [19]. However, there are only a few examples known for these less usual multiferroic mechanisms rendering the search for new materials most interesting.

Aegirine ($NaFeSi_2O_6$) belongs to the pyroxenes with general formula AMX_2O_6 (A =monovalent or divalent metal, M = divalent or trivalent metal, X= Ge or Si). It crystallizes in the monoclinic space group $C2/c$ (see Fig. 1). Crystal specimen of aegirine from nature usually shows slight compositional deviation from the ideal formula $NaFeSi_2O_6$ due to the natural doping. Natural aegirine was discovered to be multiferroic by Jodlauk *et al.* a few years ago [20]. In small crystals of natural aegirine antiferromagnetic (AFM) order sets in at 8.2 K and an additional anomaly at 6.1 K can be observed in the susceptibility data as well as in other macroscopic measurements. This second magnetic transition is accompanied by the development of spontaneous electric polarization along the monoclinic b direction $P_b \approx 13\mu C/m^2$. The electric polarization can be suppressed by a magnetic field in the ac plane, and a smaller polarization along the c direction appears instead $P_c \approx 1\mu C/m^2$ [20]. Understanding the mechanism of multiferroic coupling in aegirine requires detailed knowledge of the magnetic structure. Two investigations of the magnetic structure in aegirine based on powder neutron diffraction have been published so far [21,22]. These two publications indicate a superposition of commensurate and incommensurate magnetic order but they are contradictory and neither of them allows one to explain the origin of the spontaneous electric polarization. Muon-spin relaxation experiments on synthetic and natural samples of $NaFeSi_2O_6$ yield a different behavior for the two samples. In the synthetic sample, a single muon-oscillation frequency indicates

*Present address: Fraunhofer INT, Euskirchen, Germany.

†Present address: Max-Planck-Institut für Chemische Physik fester Stoffe, Dresden, Germany.

‡Present address : European Spallation Source, Lund, Sweden.

§braden@ph2.uni-koeln.de

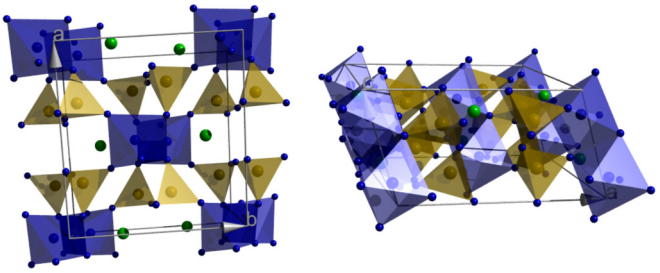

FIG. 1. (Color online) Crystal structure of natural $NaFeSi_2O_6$ at 1.8 K as determined with the single-crystal neutron diffraction experiment at *D10*. The left and right parts show views on the *ab* and *ac* planes, respectively. Blue octahedra show the FeO_6 groups and tetrahedra correspond to the SiO_4 units. Na sites are presented in green.

commensurate order, while the natural sample exhibits more complex magnetic order [23]. The symmetry breaking in $NaFeSi_2O_6$ was studied theoretically by Mettout *et al.* [24] who propose the replication of a single-order parameter as the origin of the two transitions.

In spite of considerable efforts, only one other member of the large pyroxene family was shown to exhibit multiferroic order at low temperature. Dielectric measurements on a polycrystalline sample of $NaFeGe_2O_6$ revealed a finite spontaneous ferroelectric polarization of $P \approx 13\mu C/m^2$ [25], while the more recent study on single crystals reveals a much stronger polarization of $P \approx 32\mu C/m^2$ [26], which is slightly canted out of the *ac* plane.

Here, we focus on the characterization of the magnetic structure in $NaFeSi_2O_6$ by various neutron diffraction experiments. With single crystals from the same natural piece used to analyze the multiferroic phases [20] we may establish an incommensurate magnetic structure which appears particularly interesting, as it corresponds to repeated condensation of the same irreducible representation, and as ferroelectric polarization arises from the less common $\vec{P}_{11}$ form.

II. EXPERIMENTAL

All samples of natural aegirine were cut from the same natural single crystal which was also used by Jodlauk *et al.* [20]. The chemical composition was determined to be $Na_{1.04}Fe_{0.83}Ca_{0.04}Mn_{0.02}Al_{0.01}Ti_{0.08}Si_2O_6$ by electron microprobe analysis [20]. The polycrystalline sample of synthetic $NaFeSi_2O_6$ was synthesized by crystallization of a glass of stoichiometric composition ($NaFeSi_2O_6$) at 800 °C.

Various neutron diffraction experiments were performed using unpolarized and polarized beams on $NaFeSi_2O_6$. Powder diffraction data were taken with the synthetic $NaFeSi_2O_6$ sample and with a powder obtained by grinding parts of the natural crystal using the multidetector diffractometer *G4.1* installed at the Orphée reactor ($\lambda = 2.42$Å). The sample was cooled in an Institut Laue Langevin (ILL) type liquid-helium cryostat. The first single-crystal diffraction experiments on natural $NaFeSi_2O_6$ were performed on the triple-axis spectrometer *IN3* at the ILL using a monochromatic beam with $k_i = 2.66$ Å^{-1} so that higher-order contaminations could be effectively suppressed by filters of pyrolithic graphite (PG). We used the PG monochromator and analyzer crystals of *IN3*. Large data set of nuclear and magnetic Bragg reflection intensities were collected on the *D10* diffractometer at the ILL with a wavelength of 2.36 Å using a helium cryostat. Polarized neutron diffraction experiments were performed with the *IN14* spectrometer and the CRYOPAD setup for spherical neutron polarization. We used a PG monochromator to define $k_i = 1.55$ Å^{-1} in the incoming beam which was polarized with a bender. In the outgoing beam, the neutron polarization was analyzed with a Heusler crystal yielding high precision (flipping ratio of 18 measured on a nuclear Bragg peak). For the polarized experiment it was necessary to electrically pole the crystal by applying an external voltage of ±3000 V to a plate-shaped crystal of 4.2 mm thickness yielding an electric field of ±714 V/mm. In order to apply the high voltages and to control the temperature, the amount of exchange gas in the ILL-type cryostat had to be carefully adjusted as described in previous experiments aiming at the switching of multiferroic domains [27,28]. Another experiment on natural $NaFeSi_2O_6$ was performed with the *4F2* triple-axis spectrometer at the Orphée reactor. We used a neutron beam with $k_i = 1.55$ Å^{-1} obtained with a double PG monochromator and PG analyzer. The sample was inserted in a He-gas pressure cell that allows to apply hydrostatic pressure up to 5 kbar. The pressure cell was cooled with an ILL-type liquid-helium cryostat.

III. COMMENSURATE AND INCOMMENSURATE MAGNETIC ORDER IN $NaFeSi_2O_6$

A. Unpolarized neutron diffraction experiments on natural single crystals of $NaFeSi_2O_6$

Using the *IN3* spectrometer magnetic superstructure reflections were searched by scanning along main symmetry directions in $NaFeSi_2O_6$ at 2 K with the natural single crystal. Magnetic Bragg peaks were found at many places in the $a^\star b^\star$ and $b^\star c^\star$ planes. All of them can be indexed with a single incommensurate propagation vector $\vec{k}_{inc} = (0, \sim 0.78, 0)$. Temperature-dependent scans along $(1, \xi, 0)$ are shown in Fig. 2 and the peak height, incommensurability, and correlation length of this signal are presented in Figs. 3(a)–3(c). Note that (1, 0, 0) and (0, 1, 0) are not lattice vectors in the *C*-centered lattice of $NaFeSi_2O_6$. By scanning across these magnetic Bragg peaks in the directions perpendicular to $\vec{k}_{inc}$ we can exclude a sizable incommensurate modulation in the $a^\star$ and $c^\star$ directions. The incommensurate modulation as obtained by the description with Lorentzian profiles changes very little with temperature below T_N, but the position of the diffuse scattering persisting above T_N varies considerably. The temperature dependence of the magnetic scattering at these Bragg positions agrees with the two magnetic transitions reported in the macroscopic studies revealing two magnetic transitions at about 8.2 and 6.1 K [20]. The low-temperature transition is visible as a kink in the temperature dependence of the magnetic scattering intensity registered at various positions. Furthermore, the analyzed magnetic Bragg reflections exhibit a different relative temperature dependence [see Fig. 3(d)], indicating that different magnetic components contribute to the two magnetic phases. The two magnetic transitions are not perfectly sharp but seem considerably broadened as a

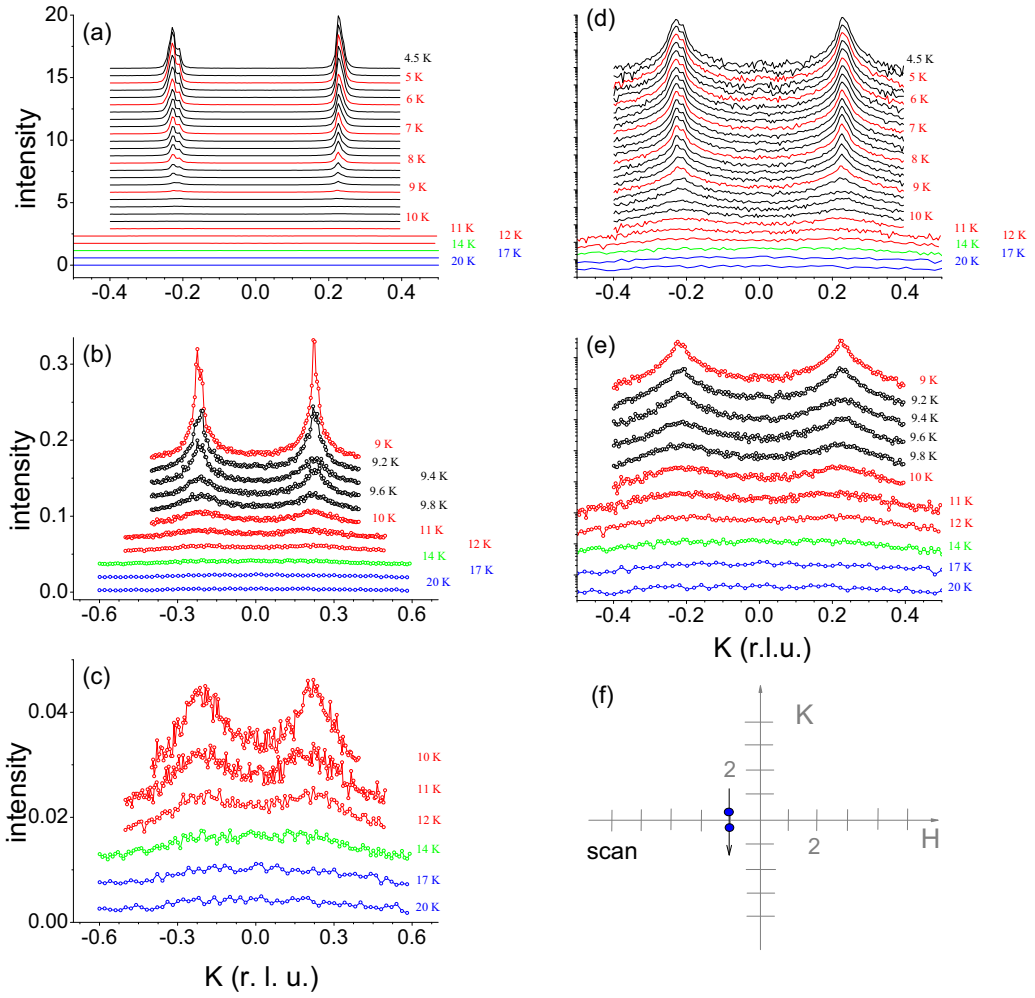

FIG. 2. (Color online) (−1 K 0) scans taken at various temperatures with the natural crystal of $NaFeSi_2O_6$ on the *IN3* spectrometer. (a)–(c) show the measured intensities in a linear scale with a constant offset between different temperatures. (b) and (c) show only the high-temperature data, in order to illustrate the scattering persisting above the Néel temperature. (d) and (e) show the same data in a semilogarithmic scale which illustrates the finite correlation lengths and diffusive scattering persisting to low temperatures. (f) Scheme of the reciprocal space plane with the scan direction; note that (−1 0 0) is not a Bragg peak in the *C*-centered lattice of $NaFeSi_2O_6$.

consequence of the structural disorder in this natural sample. Furthermore, the longitudinal correlation length strongly increases already above the upper magnetic transition [see Fig. 3(c)]. Compared to the macroscopic studies on a smaller crystal, the neutron diffraction experiments indicate a slightly larger upper $T_N = 9.0(3)$ K whose precise determination suffers from the broadened character of the transition. Diffuse magnetic scattering can be detected until 20 K, i.e., up to twice the Néel temperature, suggesting a low-dimensional or frustrated character again in agreement with the macroscopic susceptibility [20].

B. Spherical neutron polarization analysis of the magnetic structure in natural $NaFeSi_2O_6$

The triple-axis spectrometer *IN14* at ILL was used to investigate the magnetic structure of natural $NaFeSi_2O_6$ with spherical polarization analysis. A single-crystal sample of natural aegirine was mounted in the $a^\star b^\star$ scattering plane. The low-temperature propagation vector of this sample is $\vec{k}_{\rm inc} = (0,0.79,0)$. An electric field of 714 V/mm was applied parallel to the b direction during the cooling process in order to produce a monodomain state.

Polarized neutron diffraction is well suited to analyze complex magnetic structures as different components and a possible chiral contribution can be directly measured. The intensity of a neutron scattering experiment is determined by the Fourier components of the magnetization density $\vec{M}$ [29], but only components perpendicular to the scattering vector $\vec{M}_\perp$ contribute in general. In an unpolarized experiment, the intensity is just proportional to $|\vec{M}_\perp|^2 = |M_y|^2 + |M_z|^2$. We use the right-handed, orthogonal coordinate system, which is commonly considered in neutron polarization analysis [29]: $-\vec{x} \parallel \vec{Q} = \vec{k}_{\rm i} - \vec{k}_{\rm f}$, $\vec{z}$ vertical to the scattering plane, and $\vec{y} = \vec{z} \times \vec{x}$. The polarization analysis adds additional selection rules. For example, in the longitudinal channels (i.e., incoming and outgoing neutron polarization are parallel or antiparallel) magnetic contributions appear in the spin-flip (SF) channels

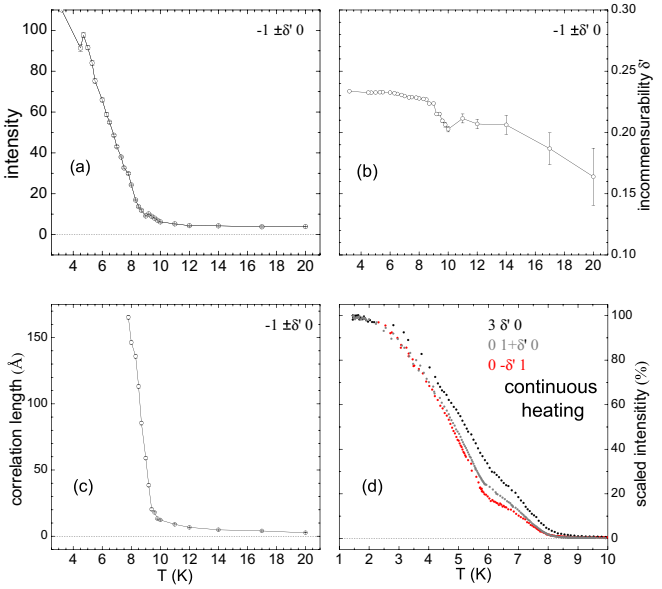

FIG. 3. (Color online) (a) Peak intensity, (b) incommensurability δ', and (c) correlation length obtained from the $(-1\ \mathrm{K}\ 0)$ scans on natural $NaFeSi_2O_6$ presented in Fig. 2 by fitting Lorentzian profiles. (d) Peak intensities at various magnetic Bragg peaks illustrating the two magnetic transitions and the different behavior arising from the different geometry factors. These intensities were recorded by continuously heating the sample crystal while counting at the peak position, which results in a slight temperature offset.

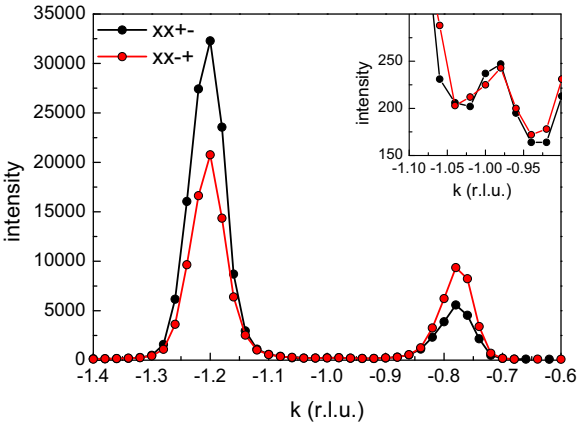

FIG. 4. (Color online) Control of chiral and multiferroic domains in the natural crystal of $NaFeSi_2O_6$ by applying an external electric field of -714 V/mm upon cooling through the magnetic transitions. For incoming and outgoing neutron polarization direction along the x direction, the two spin-flip processes corresponding to scattering from up to down and from down to up were measured. One recognizes that the majority chiral domains contribute to different neutron spin-flip channels for $\vec{Q} = (0, -1 \pm 0.21, 0)$ and that the poling of the chiral domains is not perfect ($T = 1.5$ K). The inset shows that a very small signal at the commensurate position is not chiral.

if the contribution is perpendicular to the direction of polarization, while they appear in the non-spin-flip (NSF) channel for the parallel case. Because the neutron is a chiral object when the polarization is parallel $\vec{k}$, it is not astonishing that chiral contributions defined by $M_\chi^2 = -\mathrm{i}(\vec{M}_\perp \times \vec{M}_\perp^*)_x$ can be directly studied. In the case of an ideal helix with the scattering vector parallel to the propagation vector of the helix, we may assume $\vec{M}_\perp = (0, m, \mathrm{i}m)$ with real m so that the chiral scattering is of the same size as $|\vec{M}_\perp|^2 = 2m^2$. In the xx SF channels one obtains the total intensity $\vec{M}_\perp \cdot \vec{M}_\perp^* \mp \mathrm{i}(\vec{M}_\perp \times \vec{M}_\perp^*)_x$ where the two signs correspond to the two neutron spin-flip processes from up to down or from down to up scattering. In this case of the ideal monodomain helix the total magnetic scattering would appear in one xx SF channel while the other is fully suppressed. One may thus use the comparison of the two xx SF channels in order to determine the chiral components and domains [27,28,30]. The two scans in Fig. 4 taken with these two polarization configurations after cooling in an external electric field indeed show sizable differences, which are reverted when passing from $\vec{Q} = (0, -1.21, 0)$ to $(0, 0.79, 0)$. This measurement unambiguously documents that the magnetic structure in natural $NaFeSi_2O_6$ is chiral at low temperature. The chiral ratios are, however, much smaller than 1, which together with the detailed analysis of the magnetic structure described below, indicate that natural $NaFeSi_2O_6$ cannot be poled in a monodomain state with the available range of electric fields. For example, in $MnWO_4$ [27] or in $TbMnO_3$ [30], much larger scattering ratios and nearly monodomain states were obtained. The scan in Fig. 4 also reveals a three orders of magnitude weaker commensurate signal which is not chiral.

Figure 5 shows the temperature dependence of the polarized neutron diffraction at $\vec{Q} = (0, -1.21, 0)$. One may distinguish the two transitions and the different behavior of the various SF and NSF channels which again indicate the emergence of different magnetic components in the two phases. The chiral scattering is only seen in the lower AFM phase. Aside from the xx channel, the transverse zx and yx channels also give a direct insight to the chiral magnetism because chiral contributions rotate the neutron polarization towards the x direction [29]. The measurements in the xx, zx, and yx channels perfectly agree with each other and clearly indicate that natural $NaFeSi_2O_6$ first passes into a nonchiral phase at about 9 K and that chiral components appear at about 6 K.

Figure 6 shows two temperature-dependent scans at the magnetic reflections $\vec{Q} = (0, -1.21, 0)$ and $(3, 0.21, 0)$. The data were analyzed to directly display the different magnetic contributions: $|\vec{M}_\perp|^2 = |M_y|^2 + |M_z|^2$ and $M_\chi^2 = -\mathrm{i}(\vec{M}_\perp \times \vec{M}_\perp^*)_x$. The crystal is mounted with its crystallographic c axis being vertical, i.e., $c \parallel z$. For the scan at $\vec{Q} = (0, -1.21, 0)$ we get $x \parallel b$ and $y \parallel a^*$ (approximately $y \parallel a$) and thus $M_z = M_c$ and M_y perpendicular to b and c ($M_y = M_{a^*}$). So, the intensity must arise from a magnetic moment distribution which has components in the ac plane. Note that in the monoclinic structure there is no restriction on the directions of the moments in the ac plane, see also the following. Qualitatively, we may deduce that a moment near c appears at the upper transition and an additional moment near a characterizes the lower transition. Repeating the same analysis for the reflection $\vec{Q} = (3, -0.21, 0)$ we get $x \parallel a^*$ (approximately) and $y \parallel b$ (approximately) and thus $M_z = M_c$ and $M_y \sim M_b$. The fact that there is almost no intensity for M_y indicates that there is

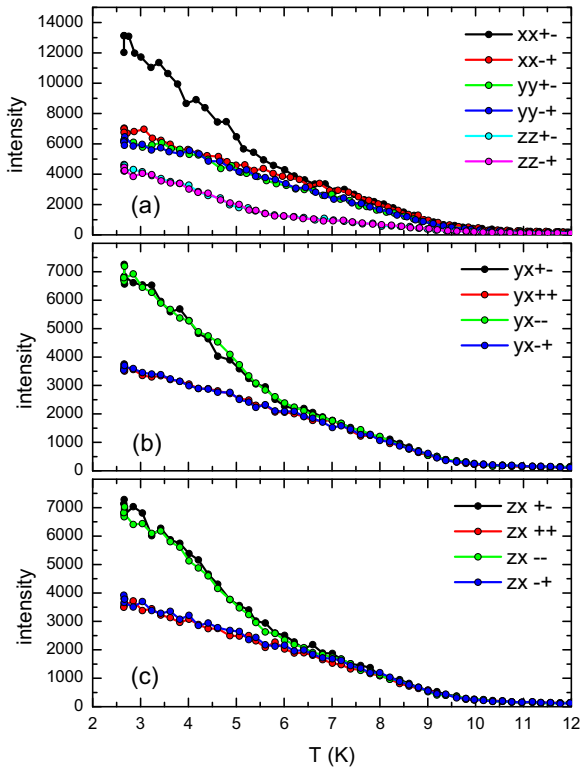

FIG. 5. (Color online) Spherical polarization analysis of the magnetic scattering at $\vec{Q} = (0, -1.21, 0)$ in natural aegirine. (a) Intensities in the two neutron spin-flip channels in the three longitudinal configurations of incoming and outgoing polarization xx, yy, and zz. ud and du designate neutron scattering processes with spin flip from up to down, and from down to up polarization, respectively. (b) The four neutron polarization channels for incoming polarization along $\pm y$ and outgoing polarization along $\pm x$ denoted by u and d are shown. Note that chiral components can rotate the neutron polarization from the y to the x direction, as it can be clearly observed. (c) The same four channels for the zx configuration. (a) and (c) were measured after poling the crystal in an external electric field of -714 V/mm, while for the data in (c) the opposed field was applied.

little or no moment parallel b (half of the small contribution in this channel is explained by the small but finite angle between $\vec{Q}$ and $\vec{a}^*$ and by the finite flipping ratio). In view of the question about the multiferroic mechanism in natural

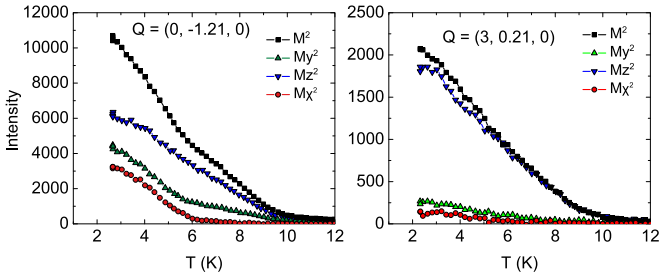

FIG. 6. (Color online) Spherical polarization analysis of magnetic intensities in natural $NaFeSi_2O_6$ recorded at *IN14*. The raw data are analyzed to directly display the different magnetic contributions. For $\vec{Q} = (0, -1.21, 0)$, we get $M_z = M_c$ and $M_y = M_{a^*}$. For $\vec{Q} = (3, -0.21, 0)$, we get $M_z = M_c$ and $M_y \approx M_b$.

TABLE I. Character table, symmetry conditions, and resulting magnetic space groups of $C2/c$ for the case of a commensurate propagation vector $\vec{k} = (0,1,0)$. Fe is situated at $(0, y, \frac{1}{4})$.

		1	2	$\bar{1}$	c	x,y,z	$\bar{x},\bar{y},\bar{z}$
Γ_1	$C2/c$	1	1	1	1	$0,v,0$	$0,v,0$
Γ_2	$C2/c'$	1	1	-1	-1	$0,v,0$	$0,\bar{v},0$
Γ_3	$C2'/c'$	1	-1	1	-1	$u,0,w$	$u,0,w$
Γ_4	$C2'/c$	1	-1	-1	1	$u,0,w$	$\bar{u},0,\bar{w}$

$NaFeSi_2O_6$, the possible existence of a chiral contribution with b and c moments is most interesting. The small chiral contribution M_χ^2 in the right panel of Fig. 6, however, can be entirely attributed to the finite flipping ratio.

Based on this qualitative analysis, the following model for the magnetic structure of natural aegirine is proposed: The magnetic moments lie mainly within the ac plane. The emergence of the chiral term M_χ^2 further indicates a helical spin-spiral structure below 6 K and a spin-density wave above.

Attempts to reverse the sign of the chiral magnetic term M_χ^2 by varying the electric field at constant temperature did not succeed at all, which seems to reflect the difficulties in poling natural $NaFeSi_2O_6$ in the field-cooling procedure. It seems likely that the disorder present in this natural material yields a strong pinning potential and slow relaxation of multiferroic domains.

C. Symmetry analysis

The crystallographic space group of $NaFeSi_2O_6$ is $C2/c$ [21]. The symmetry elements of this space group are $1, 2, \bar{1}$, and c combined with the translation t by (0.5 0.5 0). The magnetic moments are located at the Fe sites which have the special Wyckoff position $(0, y, \frac{1}{4})$; the site symmetry is a twofold rotation axis. So, the eight symmetry elements generate only four Fe sites, two of them being generated by the C centering. The magnetic moment of the latter is determined by the propagation vector yielding the phase factor of $e^{-i2\pi\vec{k}\cdot\vec{t}}$ with $\vec{k}$ the propagation vector and $\vec{t}$ the C-centered translation.

As it will be shown in the following, the synthetic sample shows magnetic reflections which can be indexed with a propagation vector $\vec{k} = (0,1,0)$ which is symmetrically equivalent to $\vec{k} = (1,0,0)$ in the C-centered lattice. For this propagation vector, the little group is identical to the space group, i.e., all symmetry operations are compatible with the propagation vector and the orbit of all atom sites is *not* split. The character table and the corresponding symmetry conditions for the magnetic moments are given in Table I. With a propagation vector $\vec{k} = (0,1,0)$ only simple AFM spin arrangements are possible. The nearest-neighbor Fe sites within a chain exhibit AFM alignment for Γ_2 and Γ_4 and ferromagnetic (FM) alignment for Γ_1 and Γ_3, respectively. With the monoclinic symmetry, one may distinguish between moments along the b direction and moments in the ac plane. The symmetry analysis was done with *BasIreps* in the FULLPROF package [31].

The magnetic propagation vector found in the natural crystal of $NaFeSi_2O_6$ is $\vec{k} = (0, \sim 0.78, 0)$. The little group contains only the elements 1 and 2 combined with the

TABLE II. Character table and symmetry conditions of the little group $G_{\vec{k}} = C2$, for the incommensurate propagation vector $\vec{k}_{\rm inc} = (0,0.77,0)$.

		1	2	x,y,z
Γ_1	$C2$	1	1	$0,v,0$
Γ_2	$C2'$	1	-1	$u,0,w$

translation t and corresponds thus to the space group $C2$. The four Fe sites belong to one orbit (i.e., they are connected by the symmetry operations) in $C2/c$, but the little group contains less symmetry elements. Therefore, the orbit splits into two orbits. With respect to the little group the two Fe sites, which are not related by the C centering (symmetry element t), are independent within the representation theory. The character table and the symmetry restrictions for the magnetic moments are given in Table II. There are two irreducible representations Γ_1 and Γ_2 which only separate the ac and b aligned moments. Note, however, that the representation theory does not fix moments and phases between the two orbits; therefore, Γ_2 can be associated with a noncollinear structure with moments in the ac plane [32].

The reflection (0,0.77,0) exhibits strong neutron scattering intensity, therefore, the irreducible representation cannot be Γ_1. In Γ_1 the magnetic moment is parallel $\vec{b}$ and for the reflection (0,0.77,0) the scattering vector $\vec{Q}$ is parallel to the magnetic moment and thus the intensity would be suppressed.

D. Refinement of the magnetic structure with single-crystal data taken on a natural sample

The magnetic structure of a single-crystal sample of natural $NaFeSi_2O_6$ was investigated at the *D10* single-crystal diffractometer at ILL using an area detector and a wavelength of $\lambda = 2.36$ Å. Structural and magnetic peaks were recorded at 1.8 K in the multiferroic phase. The propagation vector of this sample is $\vec{k}_{\rm inc} = (0,0.78,0)$.

The refinement was done in the space group $C2/c$ with the lattice constants at 1.9 K from a powder sample (see Fig. 8): $a = 9.6618(5)$Å, $b = 8.7933(4)$Å, $c = 5.2946(2)$Å, $\beta = 107.334(3)^\circ$ (see following).

1. Crystal structure

At 1.8 K, 1027 reflections were collected out of which 340 arise from the crystal structure while the remaining 687 were reflections from the magnetic structure. 240 of the structural reflections were equivalent reflections. The area detector of *D10* sometimes collects nearby reflections. The suspicious reflections were checked individually and removed from the list if necessary. 113 valid independent reflections were used for the refinement of the crystal structure. The (weighted) internal R value was 2.8% (3.3%).

The refinement was done with isotropic temperature factors and anisotropic extinction correction (model 4 in FULLPROF). The results are listed in Table III. Refinement of the occupation of the Fe and Na sites yields full occupation at the Fe place and an excess of scattering strength at the Na site suggesting that the latter hosts some of the natural doping elements (note that Na is a weak neutron scatterer).

TABLE III. Structural parameters of natural $NaFeSi_2O_6$ at $T = 1.8$ K as determined at *D10*. The R values are $R_{F^2} = 5.9\%$, $R_{wF^2} = 5.9\%$, $R_F = 3.8\%$, $\chi^2(I) = 13.5$.

Atom	x	y	z	$U_{\rm iso}$ (Å^2)
Na	0	0.3002(11)	1/4	0.010(3)
Fe	0	0.8994(4)	1/4	0.0159(17)
Si	0.2905(6)	0.0903(6)	0.2379(9)	0.0047(18)
O1	0.1137(5)	0.0796(4)	0.1384(7)	0.0078(16)
O2	0.3595(4)	0.2551(5)	0.3041(7)	0.0101(16)
O3	0.3526(4)	0.0089(5)	0.0105(6)	0.0115(14)

2. Magnetic structure

At 1.8 K, 687 magnetic reflections were recorded. After averaging, 423 independent reflections were used for the refinement.

Different models were implemented and fitted to the data with FULLPROF. In all models, the two Fe sites which belong to the two different orbits were described by identical Fourier coefficients, only the phase $\phi_{\vec{k}}$ between those two moments was chosen variable. This condition is necessary, otherwise, the absolute moment can be split arbitrarily among both sites and convergence of the refinement cannot be reached. This constraint, however, is not too strong as both sites still have the same site symmetry and thus should have similar magnetic moments. The phase between the moments which are related by the C centering is given by $\phi_{\vec{k}} = 2\pi \cdot \vec{q} \cdot \vec{t} = 2\pi 0.39$.

A helical magnetic structure with moments in the ac plane is compatible with the irreducible representation Γ_2. An elliptical helix with moments in the ac plane was fitted to the data and, for comparison, also elliptical cycloidal spirals with moments in the ab and the bc planes, respectively, were fitted to the data. Of these three models, only the ac helix is an eligible candidate as can be learned from the R values of the three models listed in Table IV. It was also tested whether adding a b component to an ac helix would lead to better results; the improvement is, however, almost negligible and the value of the b component is small. Again, for comparison, spin-density

TABLE IV. R values of different magnetic models of natural $NaFeSi_2O_6$ fitted to the data determined at *D10* at 1.8 K. Only helices within the ac plane yield a satisfying description, while adding a small b component does not significantly improve the fit.

	Cycl. ab	Cycl. bc	Hel. ac	Hel. $ac+b$
R_{F^2}	38.2%	35.3%	17.7%	17.4%
R_{wF^2}	41.7%	41.5%	19.9%	19.8%
R_F	22.3%	20.9%	12.1%	12.1%
$\chi^2(I)$	95.3	94.0	21.7	21.5
	SDW ab	SDW bc	SDW ac	SDW abc
R_{F^2}	39.1%	37.1%	30.8%	30.7%
R_{wF^2}	43.2%	45.4%	35.4%	35.3%
R_F	24.6%	23.8%	20.9%	20.2%
$\chi^2(I)$	101.6	112.2	68.2	68.1

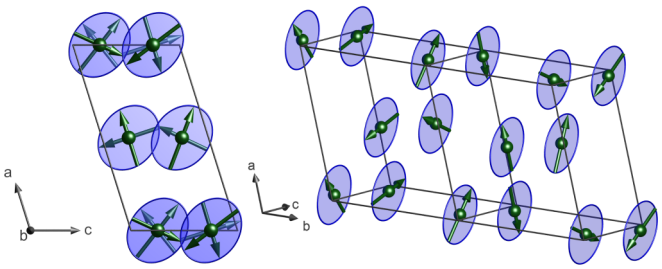

FIG. 7. (Color online) Low-temperature magnetic structure of natural $NaFeSi_2O_6$ at 1.8 K as determined at *D10*. Here, the elliptical helix with moments in the *ac* plane is pictured.

waves (SDW) in different planes were refined. SDW do not yield satisfactory results and thus can be excluded at 1.8 K.

Based on these refinements, the following model for the magnetic structure can be deduced: The low -temperature magnetic structure ($T = 1.8$ K) of the natural crystal of aegirine forms an elliptical helix with moments in the *ac* plane. The existence of a small component along *b* cannot be excluded but the refinements of the magnetic models yield no direct evidence. The lengths of the major and the minor principle axes of the basal ellipse of the helix amount to $M_{max} = 3.06(3)\,\mu_B$ and $M_{min} = 2.45(4)\,\mu_B$, $M_{min}/M_{max} = 0.80$. The angle between the major principle axis and the *c* axis amounts to $\measuredangle = 50^\circ$. The phase between the moments at the Fe sites which are related by the inversion center ($\bar{1}$) is $\phi_{\vec{k}} = 0.218(2)2\pi = 0.436(4)\pi \sim \frac{\pi}{2}$. A picture of the magnetic structure can be seen in Fig. 7.

E. Powder diffraction measurements on the natural sample

A powder sample of the same natural crystal as that used in Ref. [20] was measured in steps of 1 K from 2 K up to 11 K at the *G4.1* diffractometer at the *LLB* with a wavelength of $\lambda = 2.423$ Å. The onset of magnetic ordering can be observed around 9 K, stable refinement of the magnetic structure can be attained up to 7 K. FULLPROF [31] was used for refinement of the following magnetic models: spiral magnetic structures with moments in the *ac*, *ab*, *bc* plane and an additional model with the rotation plane tilted arbitrarily, *abc*. Spin-density waves with moments in the *ac*, *ab*, *bc* plane and in arbitrary direction *abc*. As background, a linear interpolation between a set of background points was chosen.

The various refinements confirm the magnetic structure by single-crystal diffraction: At 1.9, 3.4, and 4.2 K, a helical spiral with moments in the *ac* plane is most likely. Although, for 1.9 and 3.4 K, slightly better results are achieved when a small *b* component is added to the rotation plane of the spiral. This component, however, is small and the improvement of the magnetic *R* value is too marginal to unambiguously prove a finite *b* component. At 4.2 K, the model with the *b* component fails altogether. Near 6 K the transition from the spiral phase to the SDW can be also observed in the powder sample. At 6.1 and 7.1 K, a SDW with moments in the *bc* plane yields slightly better results than a SDW with moments in the *ac* plane. However, at that temperature the magnetic peaks are weak and broad already. Therefore (also bearing in mind the results of the measurement with polarized neutrons and the

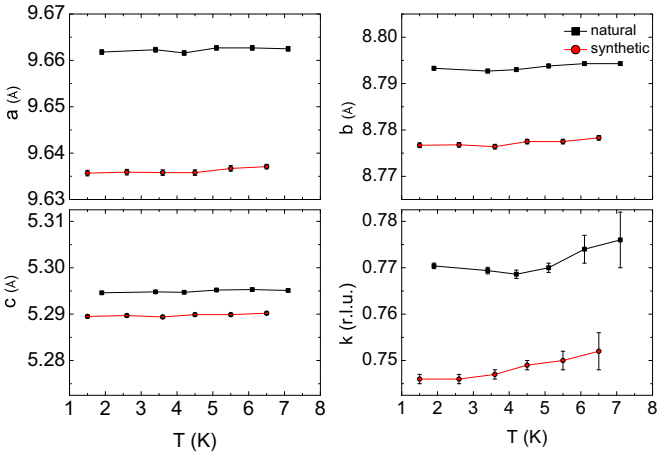

FIG. 8. (Color online) Lattice parameters and magnetic propagation vector of $NaFeSi_2O_6$ powder as determined at *G4.1*. The data displayed here correspond to the best fits, which are either a helix or a SDW with moments in the *ac* plane.

symmetry analysis), the magnetic structure in the paraelectric phase most likely forms a SDW with moments in the *ac* plane.

Figure 8 shows the lattice parameters and the propagation vector for the best fit (helix or SDW with moments in the *ac* plane). The lattice parameters show no significant temperature dependence, which was not to be expected anyway for the small temperature range. One might detect a slight increase of the propagation vector for the two highest temperatures; on the other hand, the magnetic peaks are quite weak at those temperatures and the results are not very reliable any more.

Concluding, the propagation vector of the natural powder sample is $\vec{k}_{inc} = (0,0.77,0)$. Table V shows the parameters of the magnetic structure at different temperatures for the above described models. The transition from the helix to the SDW at about 6 K can be confirmed. The data at 1.9 K and the Rietveld fit of a helical spiral with moments in the *ac* plane is shown in the upper panel of Fig. 9. There is good agreement between the powder and single-crystal results on natural $NaFeSi_2O_6$ although some details differ as it will be discussed in the following.

F. Magnetic order in synthetic $NaFeSi_2O_6$ studied by powder neutron diffraction

The incommensurate magnetic structure deduced from the single-crystal and powder neutron diffraction measurements on the natural sample fully disagree with earlier powder diffraction studies on synthetic samples which report a commensurate magnetic structure [21,22]. But, both previous studies also find incommensurate scattering at nearly the same positions as in our natural sample. In the previous studies, this scattering was discarded from the analysis [21] or treated with a most likely incorrect propagation vector [22]. In order to further elucidate the different magnetic structures in natural and synthetic samples, synthetic $NaFeSi_2O_6$ was measured at different temperatures at the *G4.1* powder diffractometer with a wavelength of $\lambda = 2.423$ Å.

Overall, the sample quality is not as good as the quality of the natural sample. There are reflections which cannot be explained by the crystal structure. These reflections are

TABLE V. Magnetic structure of natural and synthetic $NaFeSi_2O_6$ as determined by powder neutron diffraction on *G4.1*. The synthetic sample exhibits a superposition of an incommensurate and a commensurate structure while the natural sample shows only incommensurate order. The moments lie in the *ac* plane. At low temperatures, the incommensurate part forms an elliptical helix. The lengths of the major and the minor principle axes of the ellipse are denoted with M_{max} and M_{min} [μ_B]. The angle between the major principle axis and the *c* axis, $\measuredangle$, is shown. $\phi_{\vec{k}}$ is the phase between the moments at the Fe sites which are related by the inversion center ($\bar{1}$). Between 5 and 6 K, the incommensurate part of the magnetic structure evolves towards a spin-density wave. The commensurate part corresponds to parallel moments within the chains and AFM ordering in-between. Digits in parentheses refer to error bars basing on the values given by the FULLPROF program.

T (K)	M_{max}	M_{min}	$\frac{M_{min}}{M_{max}}$	$\measuredangle$ (°)	$\phi_{\vec{k}}/2\pi$	M	$\measuredangle$ (°)
Natural			$\vec{k}=(0,k,0)$			$\vec{k}=(0,1,0)$	
1.9	4.2(6)	2.5(4)	0.59	13(6)	0.21(2)		
3.4	4.1(6)	2.0(4)	0.50	16(6)	0.22(2)		
4.2	3.8(5)	1.7(4)	0.45	13(6)	0.22(2)		
5.1	3.5(4)	0.1(4)	0.03	12(6)	0.22(2)		
6.1	3.0(3)	0	0	8(6)	0.22(2)		
7.1	2.8(3)	0	0	5(6)	0.22(2)		
Synthetic							
1.5	4.7(6)	1.9(4)	0.40	11(6)	0.22(2)	1.7(1)	11(8)
2.6	4.5(5)	2.0(4)	0.44	10(6)	0.22(2)	1.7(1)	9(9)
3.6	4.6(5)	1.6(4)	0.36	11(5)	0.22(2)	1.6(1)	9(8)
4.5	4.3(5)	1.8(4)	0.43	11(6)	0.22(2)	1.5(1)	13(10)
5.5	3.8(7)	1.4(3)	0.38	12(7)	0.23(2)	1.3(1)	13(12)
6.5	3.1(6)	0	0	23(9)	0.24(3)	1.2(1)	13(14)

clearly not of magnetic origin as they do not disappear in the paramagnetic regime. The following regions are excluded from the refinement: 25.7°–27.2°, 33.6°–34.4°, 38.2°–38.9°, 52.0°–54.0°, 68.0°–68.9°. We did not succeed indexing these additional peaks by simple iron-oxide phases. In addition, an x-ray diffraction pattern did not reveal any impurity phases immediately after the sample synthesis, so that small parts of the samples must have decomposed before the neutron diffraction experiment. For the analysis of the magnetic structure, this contamination is not relevant because the magnetic Bragg reflections are well separated.

In addition to the magnetic reflections which can be indexed with the same incommensurate magnetic propagation vector as that of the natural sample, the synthetic sample shows reflections which can be described by a commensurate propagation vector $\vec{k}=(0,1,0)$. Thus, the magnetic structure in the synthetic sample is a superposition of two magnetic structures. This can be seen in the enlarged diffraction patterns shown in Fig. 10. An incommensurate broadened magnetic peak can be seen near 20° 2Θ, (0, 1.23, 0), while the peak at 15° is essentially commensurate in nature, (1, 0, 0), and that at 15.8° arises from a superposition of both phases (0, 1, 0) and (1, 0.23, 0). The temperature-dependent data in Fig. 10 clearly show that the commensurate magnetic order occurs at slightly higher temperature. The powder patterns also illustrate the strong diffuse scattering in the 2Θ range 10° to 30° persisting above the Néel temperature.

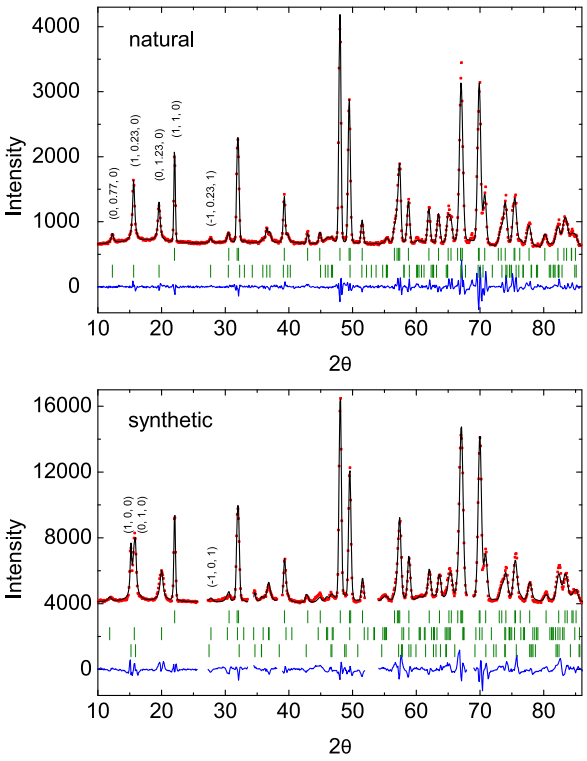

FIG. 9. (Color online) Rietveld fit of natural (1.9 K) and synthetic (1.5 K) $NaFeSi_2O_6$ powder measured at *G4.1* and refined with FULLPROF. The incommensurate magnetic structure is a helical spiral and the commensurate magnetic structure a SDW both with moments in the *ac* plane. The uppermost green ticks indicate the structural Bragg-peak positions, whereas the lower indicate the incommensurate magnetic (and commensurate for synthetic sample) Bragg-peak positions. Light red data are excluded from refinement.

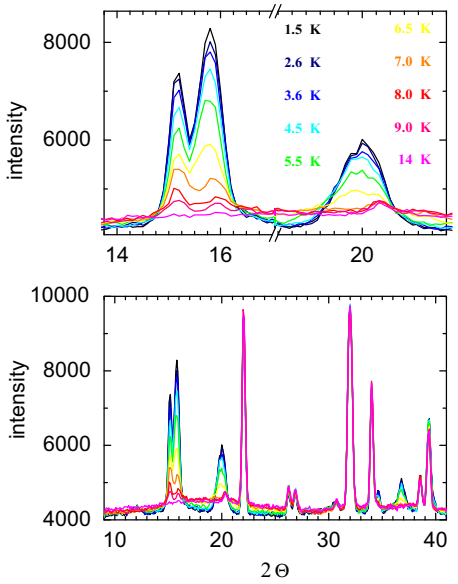

FIG. 10. (Color online) Parts of the powder neutron diffraction patterns measured with the synthetic $NaFeSi_2O_6$ sample on the *G4.1* diffractometer. The signals at 2Θ range from 15° to 16° arise from the commensurate and the incommensurate magnetic phases, and that near 20° is entirely due to the incommensurate phase (see text).

Two independent magnetic phases were fitted to the data in order to describe the incommensurate and commensurate scattering (see Figs. 9 and 10). The following magnetic models were refined with the incommensurate phase: spiral magnetic structures with moments in the *ac*, *ab*, *bc* planes and an additional model with the rotation plane tilted arbitrarily, *abc* and spin-density waves with moments in the *ac*, *ab*, *bc* planes and in arbitrary direction *abc*. The moments of the commensurate phase were restricted to the same planes as those in the incommensurate phase at each refinement, which seems to be a reasonable assumption. Due to the integer propagation vector, the moments of the second, commensurate phase are restricted to exhibit a FM alignment within the chains and AFM coupling between. The strong (1, 0, 0) commensurate magnetic peak is incompatible with an AFM coupling within the chains. The comparison of the different models confirms the previous results: at low temperature, the incommensurate magnetic structure forms a helix with moments in the *ac* plane and between 5.5 and 6.5 K it transforms into a SDW with moments remaining in the *ac* plane; the commensurate phase forms an up-down-up-down structure with moments in the *ac* plane.

Figure 8 shows the lattice parameters and the propagation vector for the best fit (helix or SDW with moments in *ac* plane plus superposition of the commensurate structure). The lattice parameters slightly increase with the temperature. One may again detect a variation of the propagation vector for the two highest temperatures at which the magnetic peaks are quite weak. Qualitatively, this behavior agrees with that observed in the single crystal [see Fig. 3(b)]. Concluding, the incommensurate propagation vector of the synthetic sample is $\vec{k}_{\rm inc} = (0, \sim 0.75, 0)$. Table V shows the parameters of the magnetic structure at different temperatures for the favored model. The transition of the incommensurate part from the helix to the SDW takes place between 5.5 and 6.5 K. The data at 1.5 K and the Rietveld fit of a helical spiral plus a superposition of the commensurate structure, both with moments in the *ac* plane, are shown in the lower panel of Fig. 9.

G. Pressure-dependent measurements at *4F2*

The previously described investigations indicate a complex magnetic structure of $NaFeSi_2O_6$ with a competition of commensurate and incommensurate order. The exact composition in the natural samples has a strong impact on the magnetic structure driving its character from commensurate to incommensurate. The different samples cut from the same larger crystal show a slight variation of the incommensurability which furthermore differs from the value found in the minority phase in the synthetic sample. It seems therefore interesting to further explore how pressure as an external parameter influences the magnetic structure in natural $NaFeSi_2O_6$.

At the triple-axis spectrometer *4F2* at the LLB the effect of hydrostatic pressure on the magnetic structure was investigated. Hydrostatic pressure up to 5 kbar was applied with a helium pressure cell. When increasing the pressure the cell must be heated above the melting point of the He. The sample was mounted in the a^*b^* scattering plane. Longitudinal scans across the magnetic peaks $\vec{Q} = (0, \sim 0.77, 0)$ and $(0, \sim 1.23, 0)$ and the commensurate position at (0,1,0) at pressures up to 5 kbar and varying temperature can be seen in Fig. 11. At zero pressure, no evidence of commensurate magnetic order can be seen with this statistics. The propagation vector $\vec{k} = (0,k,0)$ shifts to higher values with pressure and additionally the emergence of the commensurate order at (0,1,0) can be observed. The intensity of the incommensurate order decreases whereas the intensity of the commensurate order increases. It can be assumed that at slightly higher pressure, the sample exhibits completely commensurate order. This effect is reversible when going back and forth with pressure.

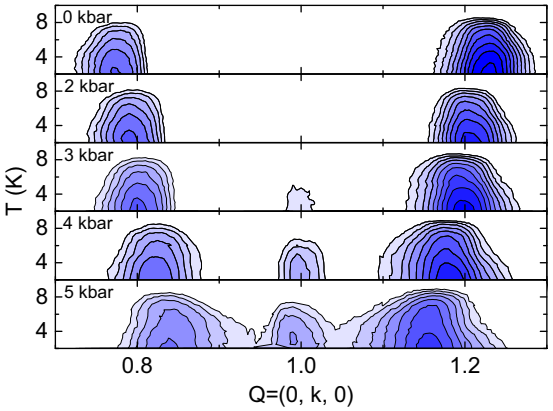

FIG. 11. (Color online) Natural $NaFeSi_2O_6$ under pressure at *4F2*. For each pressure the temperature dependency is shown in forms of contour plots. The propagation vector $\vec{k} = (0,k,0)$ shifts to higher values with pressure and the intensity of the incommensurate order decreases. Most remarkable is the onset of the commensurate order already at relatively low pressure.

A shift of the incommensurability with pressure can be expected, but this effect is very strong in $NaFeSi_2O_6$ with k varying from 0.77 at ambient pressure to 0.84 at a pressure of 5 kbar (see Fig. 10). The pressure-induced change of the character of the magnetic order from incommensurate to commensurate is further remarkable. Magnetism in $NaFeSi_2O_6$ must sense severe frustration so that a small variation of the individual interaction parameters can result in an essential change of the magnetic ground state.

IV. DISCUSSION OF THE MAGNETIC STRUCTURE AND OF THE MULTIFERROIC MECHANISM IN $NaFeSi_2O_6$

Combining the comprehensive neutron diffraction studies on natural and synthetic $NaFeSi_2O_6$, we may well characterize the magnetic structure of this multiferroic material which reacts sensitively on external parameters such as pressure or on the variation of the chemical composition.

In natural aegirine of the real composition $Na_{1.04}Fe_{0.83}Ca_{0.04}Mn_{0.02}Al_{0.01}Ti_{0.08}Si_2O_6$, magnetic order occurs upon cooling at 9 K leading to an incommensurate spin-density wave with $k = (0, \sim 0.78, 0)$ and with moments in the *ac* plane (near the *c* direction). This phase is not chiral and it does not exhibit spontaneous ferroelectric polarization. Within the FeO_6 octahedron chains running along the *c* direction, neighboring moments exhibit almost a $\pi/2$ phase shift with $\phi_{\vec{k}}/2\pi \sim 0.22$ (see Table V). This means that a full moment site in the spin-density wave has neighbors with almost vanishing moments within the chain. Therefore,

the nearest-neighbor interaction along the chains is almost inactive and cannot be taken as an important parameter in this system. The magnetism in $NaFeSi_2O_6$ cannot be described as a simple magnetic chain, as it is also suggested by incommensurate modulation emerging perpendicular to the chains. The next-nearest-neighbor interaction along the chains should be FM (see following), but will probably be much weaker than the various interchain parameters which most likely are frustrated.

Upon cooling natural aegirine below 6 K the magnetic structure transforms to an elliptical helix with moments remaining in the *ac* plane. This magnetic structure is chiral as it is unambiguously shown by the polarization analysis. The chirality is directly connected with the ferroelectric polarization because the magnetic chirality can be poled with an external electric field. Also in this helical phase the nearest-neighbor intrachain interaction is not active as the phase between neighboring Fe moments is not essentially changing at the transition. In the helical phase, neighboring moments along the chain are thus nearly perpendicular. It is remarkable that the second magnetic transition in natural $NaFeSi_2O_6$ is described by the same irreducible representation of the paramagnetic group; the helical transition is thus a repetition of the same scheme [24], but similar cases are known [32].

The third magnetic phase we find in $NaFeSi_2O_6$ only appears in the synthetic sample where it forms the minority magnetic phase. This magnetic structure is commensurate with a propagation vector of $\vec{k} = (0,1,0)$ which signifies that the moments in two chains translated by (0.5, 0.5, 0) are antiparallel. Within the chains we find parallel alignment similar to the case of the commensurate magnetic order in $LiFeSi_2O_6$ [33]. The different intrachain arrangements and the different propagation vectors seem to result from a fine balance of frustrated interaction parameters acting between the chains.

The low-temperature magnetic propagation vector of different samples cut from the same natural crystal of $NaFeSi_2O_6$ [20] varies between (0,0.77,0) to (0,0.79,0). The frustrated nature of the magnetic structure results in strong sensitivity on external parameters as the exact composition of the sample. It is likely that the exact composition varies slightly throughout the large natural crystal, which may also induce some variation in the transition temperature. The strong influence of external parameters on the propagation vector can also be observed when pressure is applied to the sample: the propagation vector shifts to higher values for increasing pressure (compare Fig. 11). The temperature dependence of the propagation vector is, however, marginal within the ordered phases at constant pressure (compare Figs. 3, 8, and 11).

The size of the ordered magnetic moment at 1.8 K derived with the single-crystal diffraction data amounts to $3.06\,\mu_B$. The powder diffraction experiments reveal a slightly larger magnetic moment and a flatter ellipse, while the angle between the major axis and the *c* axis is smaller. These discrepancies may arise from the large parameter space to be refined. While single-crystal diffraction does not suffer from peak overlap, extinction effects can influence the scaling of the magnetic phase with single-crystal data and thus compromise the determination of the moments. The theoretical magnetic moment of Fe^{3+} amounts to $5.92\,\mu_B$. The significant discrepancies indicate that the magnetic moments are not completely ordered in the natural sample. The reason for that might be the high frustration of the magnetic structure combined with the significant amount of disorder induced by the chemical impurity, which also dissolves the magnetic lattice. The coexistence of two magnetic phases in the synthetic sample impairs the quantitative determination of the ordered moment therein, but qualitatively the total ordered moment seems to exceed that in the natural sample.

The pressure experiment at *4F2* reconciles the different behaviors of the synthetic and natural samples. By applying relatively low pressure up to 5 kbar on a natural sample it is possible to essentially alter and finally suppress the incommensurate magnetic structure regaining the commensurate order observed in synthetic $NaFeSi_2O_6$. The low-pressure change of the propagation vector approaches the commensurate one, so that the same underlying variation of interaction energies can explain both effects. The magnetic structure in $NaFeSi_2O_6$ is frustrated, therefore, external parameters such as doping and pressure can take great influence on the propagation vector.

Considering the purely helical character of the magnetic structure in multiferroic $NaFeSi_2O_6$ we can exclude the inverse DM interaction [3] as the driving magnetoelectric coupling. This mechanism requires some cycloidal character or in other words some rotation of the spiral plane towards parallel to the propagation vector. The magnetic refinements and the neutron polarization analysis do not give any evidence for such an effect. However, the alignment of the propagation vector of the helix parallel to the twofold axis of this monoclinic structure breaks inversion symmetry and allows for a finite polarization parallel to the twofold axis, as it was first proposed by Arima [17]. This can be easily understood because rotating a moment from, e.g., the *c* direction towards $+\vec{a}$ or $-\vec{a}$ is different in the monoclinic system. Amongst the general biquadratic spin forms basing on spin canting [14], $\vec{P}_{II} \propto (\vec{S}_i \times \vec{S}_j)$ can perfectly describe the orientation of the ferroelectric polarization parallel to the *b* direction. This form is allowed in $NaFeSi_2O_6$ due to its low monoclinic symmetry. Natural $NaFeSi_2O_6$ is thus a rare example of a multiferroic material in which ferroelectric polarization does not arise from the common $\vec{P}_I \propto \vec{r}_{ij} \times (\vec{S}_i \times \vec{S}_j)$ mechanism.

V. CONCLUSION

By comprehensive neutron diffraction studies on natural and synthetic $NaFeSi_2O_6$, we determine its magnetic structure in various phases. In natural $NaFeSi_2O_6$, which contains a significant amount of natural doping, magnetic order sets in around 9 K forming a spin-density wave with an incommensurate propagation vector parallel to the monoclinic axis. Upon further cooling below 6 K, a transition into a helical structure occurs that is accompanied by the onset of spontaneous ferroelectric order. The ferroelectric polarization appears along the propagation vector which cannot be explained by the most common mechanism basing on the inverse Dzyaloshinski-Moriya interaction. Instead, the spontaneous polarization is well described by $\vec{P}_{II} \propto (\vec{S}_i \times \vec{S}_j)$ which can cause a macroscopic polarization in $NaFeSi_2O_6$ due to its low monoclinic symmetry. The two magnetic transitions in $NaFeSi_2O_6$ correspond to a repeated condensation of an order parameter belonging to the same irreducible representation.

The magnetic structure in $NaFeSi_2O_6$ can be significantly modified by varying the chemical composition or by applying external pressure. Synthetic $NaFeSi_2O_6$ exhibits coexistence of the similar incommensurate magnetic order as described above with commensurate order. Apparently, frustration of magnetic interaction results in a strong sensitivity of the magnetic ground state on minor modifications. Applying external pressure on natural $NaFeSi_2O_6$, we first observe a strong variation of the incommensurate propagation vector and finally a transition towards commensurate order which starts at only 3 kbar but which stays incomplete at 5 kbar.

ACKNOWLEDGMENT

This work was supported by the Deutsche Forschungsgemeinschaft through the Sonderforschungsbereich 608.

[1] W. Eerenstein, N. D. Mathur, and J. F. Scott, Nature (London) **442**, 759 (2006).
[2] S.-W. Cheong and M. Mostovoy, Nat. Mater. **6**, 13 (2007).
[3] H. Katsura, N. Nagaosa, and A. V. Balatsky, Phys. Rev. Lett. **95**, 057205 (2005); M. Mostovoy, *ibid.* **96**, 067601 (2006); I. A. Sergienko and E. Dagotto, Phys. Rev. B **73**, 094434 (2006).
[4] T. Kimura, T. Goto, H. Shintani, K. Ishizaka, T. Arima, and Y. Tokura, Nature (London) **426**, 55 (2003).
[5] G. Lawes, A. B. Harris, T. Kimura, N. Rogado, R. J. Cava, A. Aharony, O. Entin-Wohlman, T. Yildirim, M. Kenzelmann, C. Broholm, and A. P. Ramirez, Phys. Rev. Lett. **95**, 087205 (2005).
[6] K. Taniguchi, N. Abe, T. Takenobu, Y. Iwasa, and T. Arima, Phys. Rev. Lett. **97**, 097203 (2006).
[7] O. Heyer, N. Hollmann, I. Klassen, S. Jodlauk, L. Bohatý, P. Becker, J. A. Mydosh, T. Lorenz, and D. Khomskii, J. Phys.: Condens. Matter **18**, L471 (2006).
[8] A. H. Arkenbout, T. T. M. Palstra, T. Siegrist, and T. Kimura, Phys. Rev. B **74**, 184431 (2006).
[9] A. Pimenov, A. Mukhin, V. Ivanov, V. Travkin, A. Balbashov, and A. Loidl, Nat. Phys. **2**, 97 (2006).
[10] H. Katsura, A. V. Balatsky, and N. Nagaosa, Phys. Rev. Lett. **98**, 027203 (2007).
[11] D. Senff, P. Link, K. Hradil, A. Hiess, L. P. Regnault, Y. Sidis, N. Aliouane, D. N. Argyriou, and M. Braden, Phys. Rev. Lett. **98**, 137206 (2007).
[12] T. Finger, K. Binder, Y. Sidis, A. Maljuk, D. N. Argyriou, and M. Braden, Phys. Rev. B **90**, 224418 (2014).
[13] R. Valdés Aguilar, M. Mostovoy, A. B. Sushkov, C. L. Zhang, Y. J. Choi, S.-W. Cheong, and H. D. Drew, Phys. Rev. Lett. **102**, 047203 (2009).
[14] T. A. Kaplan and S. D. Mahanti, Phys. Rev. B **83**, 174432 (2011).
[15] T. Moriya, Phys. Rev. **120**, 91 (1960).
[16] T. Nakajima, S. Mitsuda, S. Kanetsuki, K. Prokes, A. Podlesnyak, H. Kimura, and Y. Noda, J. Phys. Soc. Jpn. **76**, 043709 (2007).
[17] T. Arima, J. Phys. Soc. Jpn. **76**, 073702 (2007).
[18] M. Soda, K. Kimura, T. Kimura, M. Matsuura, and K. Hirota, J. Phys. Soc. Jpn. **78**, 124703 (2009).
[19] M. Kenzelmann, G. Lawes, A. B. Harris, G. Gasparovic, C. Broholm, A. P. Ramirez, G. A. Jorge, M. Jaime, S. Park, Q. Huang, A. Ya. Shapiro, and L. A. Demianets, Phys. Rev. Lett. **98**, 267205 (2007).
[20] S. Jodlauk, P. Becker, J. Mydosh, D. Khomskii, T. Lorenz, S. Streltsov, D. Hezel, and L. Bohatý, J. Phys.: Condens. Matter **19**, 432201 (2007).
[21] O. Ballet, J. Coey, G. Fillion, A. Ghose, A. Hewat, and J. Regnard, Phys. Chem. Miner. **16**, 672 (1989).
[22] G. Redhammer, A. Senyshyn, M. Meven, G. Roth, S. Prinz, A. Pachler, G. Tippelt, C. Pietzonka, W. Treutmann, M. Hoelzel, B. Pedersen, and G. Amthauer, Phys. Chem. Miner. **38**, 139 (2011)
[23] P. J. Baker, H. J. Lewtas, S. J. Blundell, T. Lancaster, I. Franke, W. Hayes, F. L. Pratt, L. Bohatý, and P. Becker, Phys. Rev. B **81**, 214403 (2010).
[24] B. Mettout, P. Tolédano, and M. Fiebig, Phys. Rev. B **81**, 214417 (2010).
[25] I. Kim, B.-G- Jeon, D. Patil, S. Patil, G. Nénert, and K. H. Kim, J. Phys.: Condens. Matter **24**, 306001 (2012).
[26] M. Ackermann, L. Andersen, T. Lorenz, L. Bohatý, and P. Becker, New J. Phys. **17**, 013045 (2015).
[27] T. Finger, D. Senff, K. Schmalzl, W. Schmidt, L. P. Regnault, P. Becker, L. Bohatý, and M. Braden, Phys. Rev. B **81**, 054430 (2010).
[28] M. Baum, J. Leist, Th. Finger, K. Schmalzl, A. Hiess, L. P. Regnault, P. Becker, L. Bohatý, G. Eckold, and M. Braden, Phys. Rev. B **89**, 144406 (2014).
[29] P. J. Brown, in *Neutron Scattering from Magnetic Materials*, edited by T. Chatterji (Elsevier, Amsterdam, 2006).
[30] Y. Yamasaki, H. Sagayama, T. Goto, M. Matsuura, K. Hirota, T. Arima, and Y. Tokura, Phys. Rev. Lett. **98**, 147204 (2007).
[31] J. Rodríguez-Carvajal, http://www.ill.eu/sites/fullprof/
[32] J. M. Perez-Mato, J. L. Ribeiro, V. Petricek, and M. I. Aroyo, J. Phys.: Condens. Matter **24**, 163201 (2012).
[33] M. Baum, K. Schmalzl, P. Steffens, A. Hiess, L. P. Regnault, M. Meven, P. Becker, L. Bohatý, and M. Braden, Phys. Rev. B **88**, 024414 (2013).